applied sciences

MDPI

Article

Advanced Elastic and Reservoir Properties Prediction through Generative Adversarial Network

Muhammad Anwar Ishak [1,2], Abdul Halim Abdul Latiff[1], Eric-Ho Tatt Wei[1], M Izzuljad Ahmad Fuad[2], Tan Nian Wei[2], Muhammad Sajid[2] and Emad Elsebakhi[2]

[1] Centre of Subsurface Imaging, Department of Geosciences, Universiti Teknologi PETRONAS, 32610 Bandar Seri Iskandar, Perak, Malaysia.
[2] PETRONAS Research Sdn Bhd (PRSB), Lot 3288 & 3289, Off Jln Ayer Itam, Kawasan Institusi Bangi, 43000, Kajang, Selangor, Malaysia.

Abstract: Prediction of the subsurface properties such as velocity, density, porosity and water saturation has been the main focus of petroleum geosciences. Advanced methods such as Full Waveform Inversion (FWI), Joint Migration Inversion (JMI) and ML-Rock Physics are able to produce better prediction than their predecessors, but they still require tedious manual interpretation which is prone to human error. Besides, the research on these methods remains open as they suffer from technical limitations. As the computing resource is becoming cheaper, the use of a single deep generative adversarial network is feasible in predicting all these properties in a completely data-driven manner. In our proposed method of multiscale pix2pix applied on SEG SEAM salt data, we have managed to map from one input which is seismic post-stack data to several outputs of reservoir and elastic properties which are porosity, water saturation, velocity and density by using only one trained model and without having to manually interpret or pre-process the input data. With 90% accuracy of the results, the method is worth to be explored by the petroleum geoscience fraternity.

Keywords: elastic & reservoir properties, velocity model building, rock physics, generative adversarial net, pix2pix

1. Introduction

Accurate prediction of the elastic and reservoir properties is crucial in getting a more precise image of the subsurface. This will lead to the correct placement of the well, reducing the risk and uncertainties thus increasing the chance of success in finding hydrocarbon. Velocity model building (VMB), and seismic inversion and rock physics study have been used to achieve these objectives. Although a significant advancement has been made on these two methods, they remain an open topic with a lot of ongoing researches. There are several approaches of VMB [1]. The most conventional method is tomography, an iterative process involving several steps such as sorting the data into common image point (CIP) and picking the reflections to flatten the image gather prior to produce the final velocity model. Another widely used approach is Full Waveform Inversion (FWI) [2] which calculates the misfit between the observed and calculated data. Traditional FWI is depth limited as the diving wave does not penetrate enough in the subsurface, hence the reflection FWI (RFWI) is proposed [3]. RFWI itself suffers from a highly non-linear coupling of the density and velocity. The problem faced by RFWI can be solved by Joint Migration Inversion (JMI) [4,5], which manages to reduce the non-linearity of the inversion. However, JMI is based on one way wave equation which is inferior to FWI. In 2018, a hybrid FWI-JMI has been proposed [6]. Seismic inversion and rock physics study is another method used in reservoir characterization. Unlike VMB, this method is much more focused in the reservoir itself rather than the entire seismic volume [7,8]. In a multi-step inversion approach, elastic properties like P-impedence, S-impedence, and density

Citation: To be added by editorial staff during production.

Academic Editor: Firstname Lastname

Received: date
Revised: date
Accepted: date
Published: date

are produced by stochastic or deterministic inversion on seismic data. Next, at a well, a rock physics model is developed connecting these elastic properties to reservoir properties. High resolution models of the reservoirs properties are created in a single loop manner before rock physics transformations are used to create the elastic properties volume. After that, calculated synthetic seismic traces are compared to actual seismic data. In order to combine these multi-step and single-loop approaches, Grana, D. [7] suggested to use the output from the first approach as an a priori for the second approach. As was previously established, inversion and rock physics are reservoir-centric, and accuracy decreases as reservoir depth increases. A regional rock physics template (RPT), which is based on the rock physics inclusion model, has been proposed to address these issues [9].

2. Related Work

AI-Velocity Model. The application of neural network for velocity model building dated back in the 1990s. Röth, G. et al [10] used neural network to predict 1D velocity from shot gathers. Similar work has recently been published [11] which maps the 1D vertical velocity profile from data cubes of neighboring common midpoint (CMP) gathers. Their work applied advanced DL architecture which is Visual Geometry Group (VGG) network and is able to accommodate lateral heterogeneity in the model, a problem faced in [12] in generalizing the neural network training by creating 4 different sets of geologically inspired geometric training models with and without background velocity gradient. The authors managed to produce plausible results with only one neural net (NN) and one fully connected (FC) layer as the network architecture. Earlier work of [13] has also shown the feasibility of the UNET architecture to approximate the non-linear mapping into the velocity model from multi shot gathers. The authors also suggested for generative adversarial network (GAN) to be used in future testing. Another example is by [12] in the paper of DL tomography which the authors applied 3 dense layers to learn the tomography operator from the seismic data. Based on the example here, most of the model building technique focus only on building the velocity model [11,12,14,15] and in certain cases, density model [16].

AI-Rock Physics. Application of machine learning or deep learning in rock physics has gained attention in recent years. One of the early applications used two simple 1D convolutional layers in solving the seismic inversion problem of predicting the elastic model of the subsurface from recorded seismic data [17]. The authors generated numerical training set of P-Impedence realizations with the corresponding seismic response and able to have a good generalize network. In another example, the convolutional neural networks (CNN) have been used to predict the reservoir properties directly in the depth domain given the time domain pre-stack seismic data [18]. The feasibility of the method was shown by comparing two CNN networks namely PetroNet (end-to-end CNN) and ElasticNet-ElasticPetroNet (cascaded CNN). Besides deriving the reservoir and elastic properties directly from the seismic data, the neural net was also tested in predicting the reservoir properties from the elastic properties [19]. Several inputs of different elastic properties were passed together into a three-layer neural net to produce the reservoir properties.

Generative Adversarial Networks. Deep learning is a subset of machine learning and machine learning itself is a subset of artificial intelligence. Generative adversarial networks or GAN [20] is a 2-network architecture which consists of a generator that produces the translated image and a discriminator that tries to classify its input whether it is generated (fake) or coming from the label set (real). GAN has become one of the best deep learning networks due to its ability to produce remarkable photorealistic results in many computers vision tasks such as image generation [20], image transformation or translation [20,21], styling [22] and super resolution [23,24]. Besides, many GAN networks were also applied in medical image segmentation [25-31]. Despite the success of GAN in both domains, the application of GAN in geosciences is however limited. Some of the applications

in geosciences are compressive sensing [32], facies classification [33] and rock type inference [34,35].

In this paper, we modified a generative deep learning (GAN) method called pix2pix proposed by Isola, P. et al [20] and applied it to a synthetic post-stack seismic data. We verified the feasibility of the method in predicting or mapping the reservoir and elastic properties directly. Firstly, the input and target data were prepared as required by the DL network. Then, we splitted the data into training/validation and testing and trained them for a number of epochs. Next, we look at the validation results and did the testing on the unseen data and finally we discussed those results, the shortcomings and the way forward of this method.

Overall, there are two main contributions of our work which are:

1. the groundwork of a new method alongside with velocity model building and rock physics to predict the subsurface properties which is entirely data-driven without any manual interactions.
2. the multiscale patchGAN which extracts features at different scale thus improves the accuracy of final predictions.

3. Pix2Pix and Multiscale PatchGAN of Pix2Pix

Pix2pix is a type of conditional GAN [20] of which the mapping of the generator, G to output, y is learnt from the observed data, x and random noise vector, z.

$$G : \{x, z\} \rightarrow y$$

G is trained to produce outputs that cannot be distinguished from label data (real) by an adversarially trained discriminator, D, which is trained to detect the generated output (fake). Both G and D are competing within each other in a min-max game which G is trying to minimize its loss by producing output as similar as possible to the true label (Fig. 1) while D is trying to maximize its "correctness" at detecting whether its incoming input is real or fake (Fig. 2) . In the original pix2pix network, G is U-NET while D is PatchGAN.

$$l_{cGAN}(G, D) = E_{x,y}[\log D(x, y)] + E_{x,z}\left[\log\left(1 - D\left(x, G(x, z)\right)\right)\right]$$

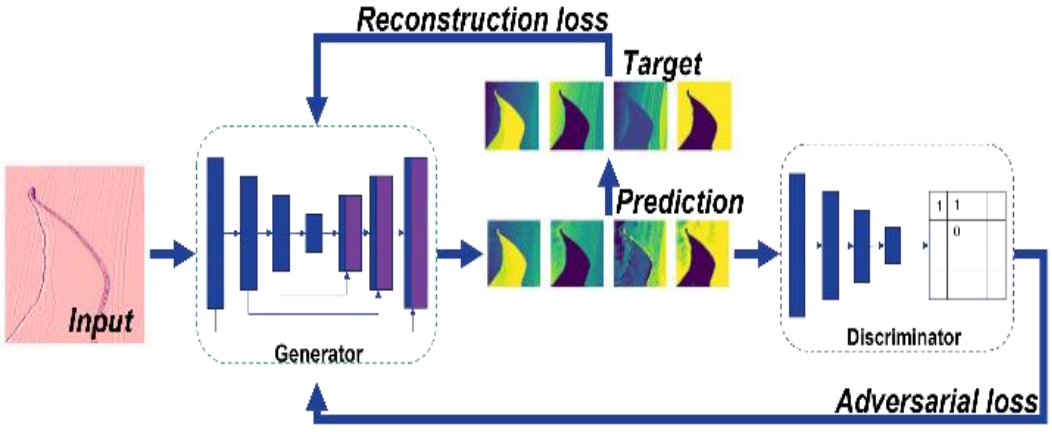

Figure 1 The diagram for the generator training. The generator loss is the sum of the reconstruction loss and the adversarial loss

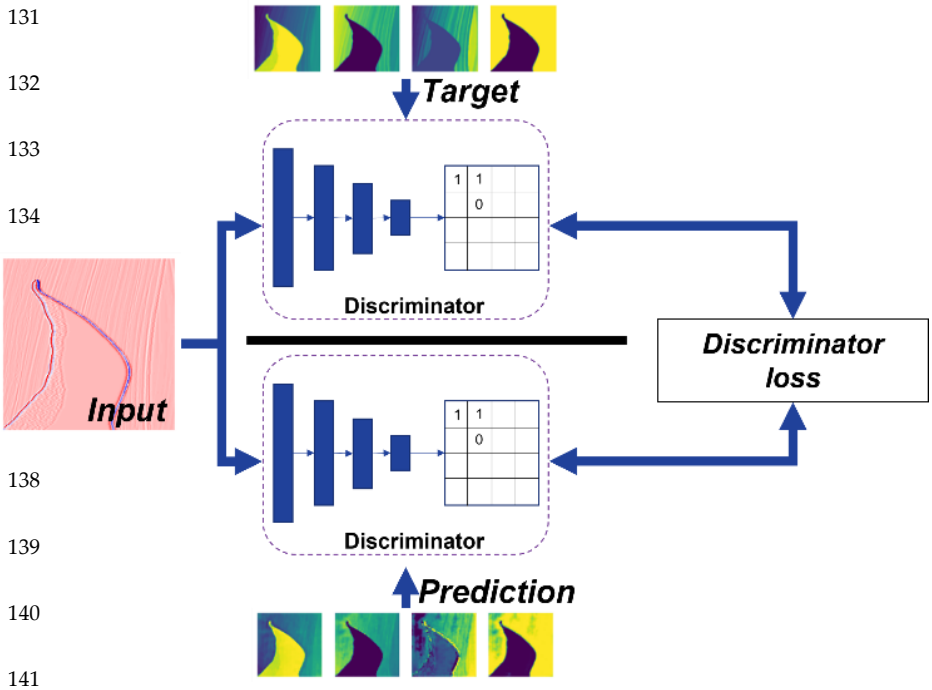

Figure 2 The diagram for the discriminator training. The discriminator loss is the sum of real loss and fake loss.

Proposed Network

The proposed network is an enhanced version of the original pix2pix. We use the original pix2pix (Fig. 3) as the base network to produce the base model and we re-train the base model with the same pix2pix architecture but with a smaller kernel size. In theory, smaller kernel size would mean high resolution feature extraction, but it cannot be too small of which there will be not enough information that the kernel can extract. The proposed solution is also based on StarGAN [21], an approach of which only a single network is trained for performing image-to-image translation of multiple domains. Such a unified model architecture allows simultaneous training of multiple datasets with different domains within a single network. We have adapted this idea in transforming the seismic data into 4 different reservoir and elastic properties by using only one model. The summary of our proposed network can be seen in the Table 1 below.

Table 1 Summary of the changes made to the original pix2pix

Parameter	Original Pix2Pix	Proposed method
Input channel	3	1
Output channel	3	4
Kernel size of G	4,4	4,4
Kernel size of D	4,4	4,4 & 3,3

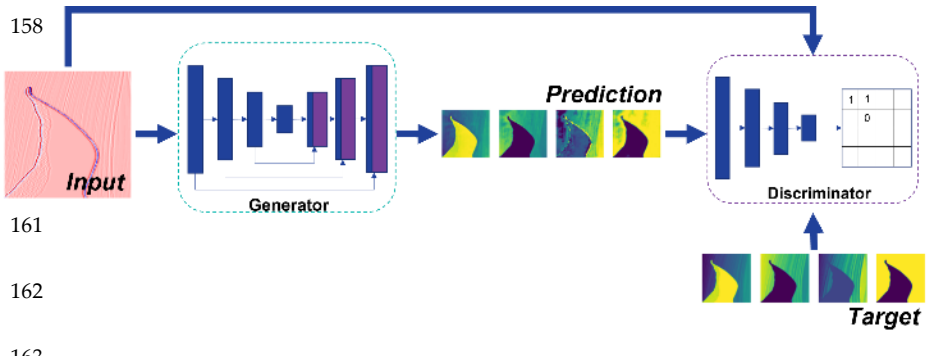

Figure 3 The original pix2pix network.

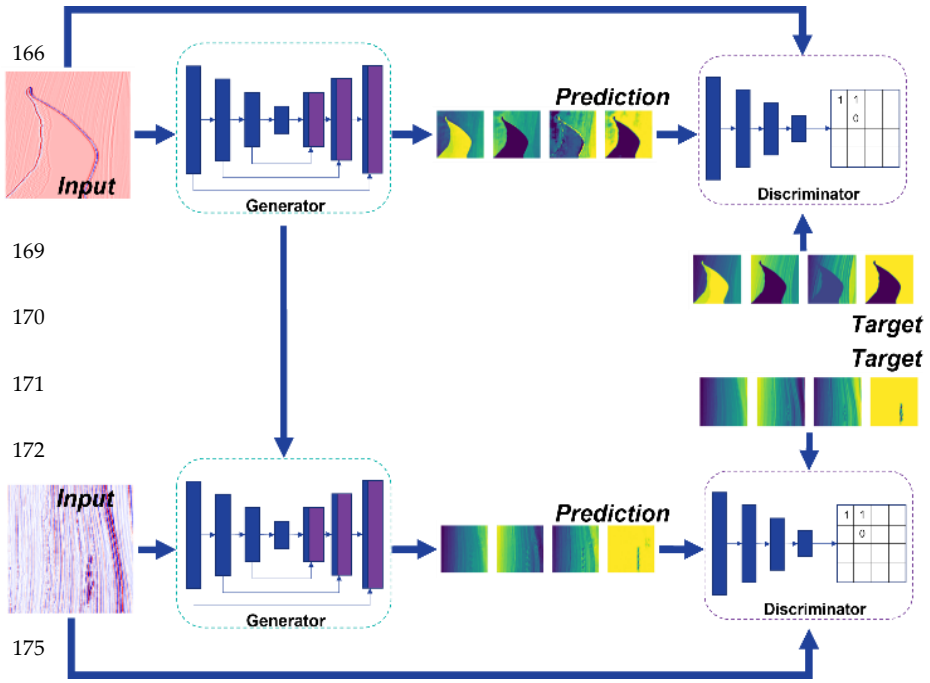

Figure 4 The architecture of the proposed method.

4. Experiments

In this section, we validate our proposed method on the SEG Seam salt dataset which is seismic post-stack, velocity, porosity, density and water saturation

A. Data preparation

Fig. 5 shows the data preparation workflow. Each of the dataset (except for porosity) is normalized to 0 and 1 range based on the property's fix values i.e. 1500 – 5000 for velocity, -0.3 – 0.3 for seismic amplitude and 1 – 5 for density. We then select 1000 inlines from each of the dataset and transform them into patches of the size 256x256. The total number of patches for each dataset is 25000. We then input the seismic data as our $\boldsymbol{x}$ and velocity, porosity, density and water saturation as our $\boldsymbol{y}$ $(\boldsymbol{y_1}, \boldsymbol{y_2}, \boldsymbol{y_3}, \boldsymbol{y_4})$ into the dataloader. We then split the dataloader to 90% training and 10% validation and input them into the network.

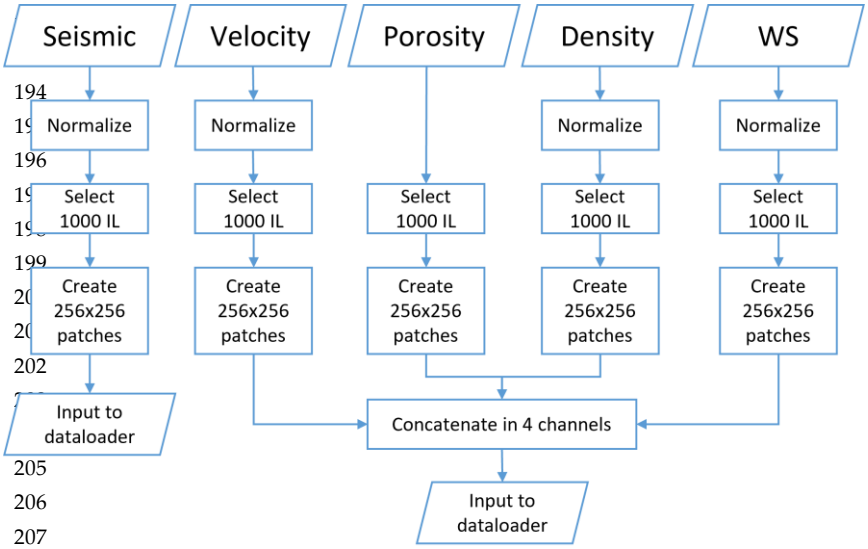

Figure 5 Data preparation workflow. Normalization from 0 to 1 is done on all dataset except for porosity as the data value is already within the normalization range

B. Training/validation

We start the training with the default pix2pix setting for up to 2000 epochs. We implement the early stopping [36] manually by doing qc on the validation results and model at every 50 epochs. The advantage of implementing early stopping is that we don't have to wait until the training is done for 2000 epochs. If we have a good intermediate model, we can stop the training early. We select the model that gives the highest validation accuracy as our base model which in this case is the model 1000 (Fig. 6).

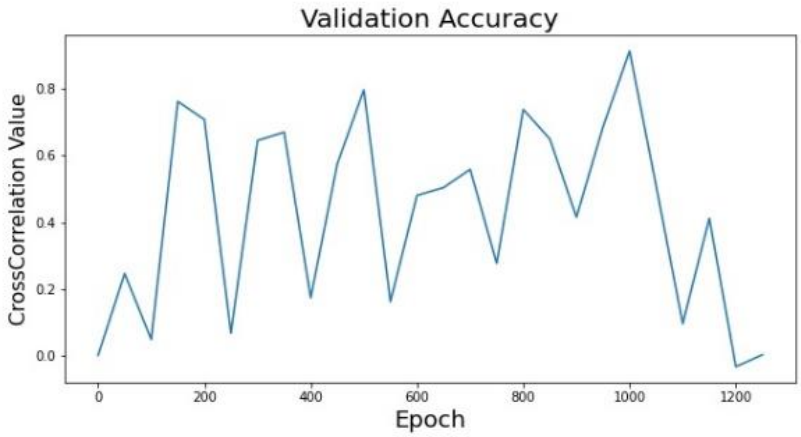

Figure 6 Validation accuracy of the training of the original pix2pix. Model 1000 is selected as our base model as it gives the highest accuracy for the validation results. Noted that we stopped the training at 1250 and not 2000 as the accuracy trend is decreasin

Next, we re-train the base model using the same number of parameters except the discriminator kernel size of which we change from 4 to 3. We implement the same early stopping strategy. Here, the best model is model 0 as it gives the highest accuracy for the validation set (Fig. 7).

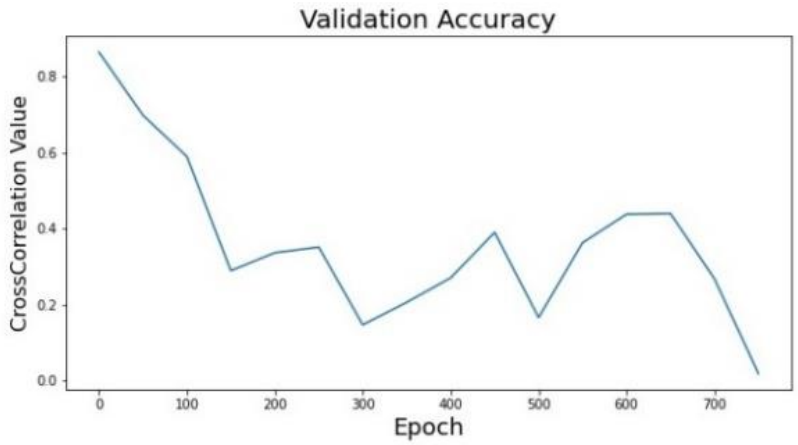

Figure 7 Validation accuracy of the second network training with different kernel size. Model 0 gives the highest accuracy.

C. Testing

Now we have our base model (pix2pix) and final model (MS-pix2pix, the proposed method), we do testing on 2 inlines that are not included during the training phase previously (Fig.8). The Inline 1 is chosen to represent an area with simple geology, layer cake strata with a small section of salt body while Inline 2 represents an area with complex geology with big section of salt body. The inlines size are 1024x1024 and we apply normalization to them before being input into both models. We compare the results of both models and also both inlines in the next section

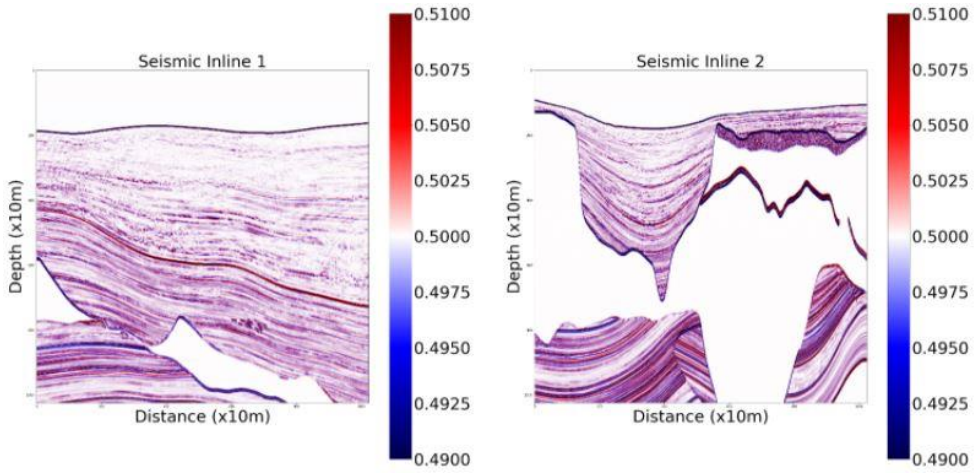

Figure 8 left: Inline 1. Simple geological section with a small salt body, right: Inline 2. Complex geological section with bigger salt body. The color bar is exaggerated to make the sections clearer

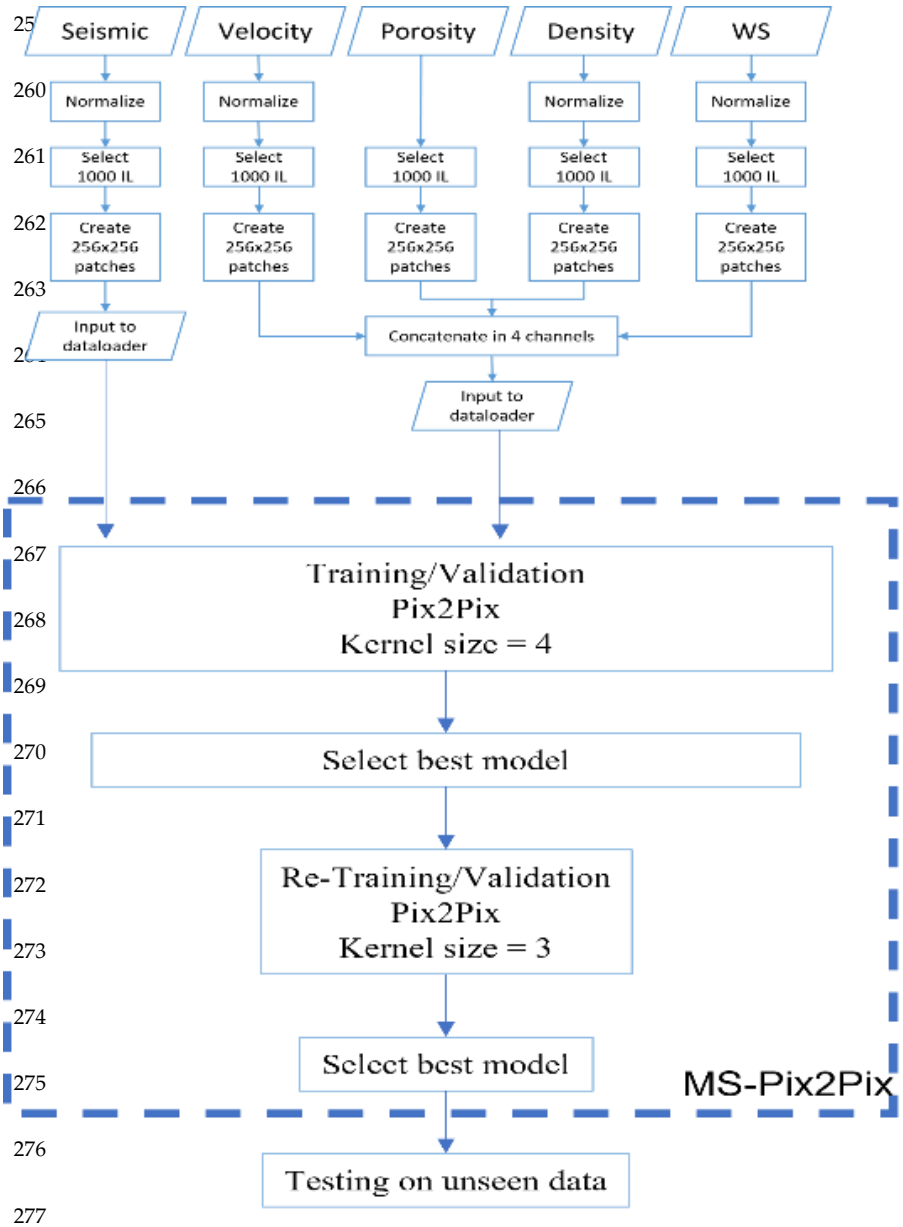

Figure 9 The complete workflow of the proposed method. The best model from the original Pix2Pix is re-trained with a different kernel size of the discriminator

5. Results and Discussion

This section is organized as follow. Each figure contains 3 images: prediction from pix2pix, prediction from MS-pix2pix (proposed method) and the ground truth. The first 2 figures are the velocity prediction for Inline 1 and Inline 2. The next 2 figures are the porosity prediction, followed by density and lastly water saturation. The accuracy metric used are cross correlation and structural similarity index, SSIM (Table 2).

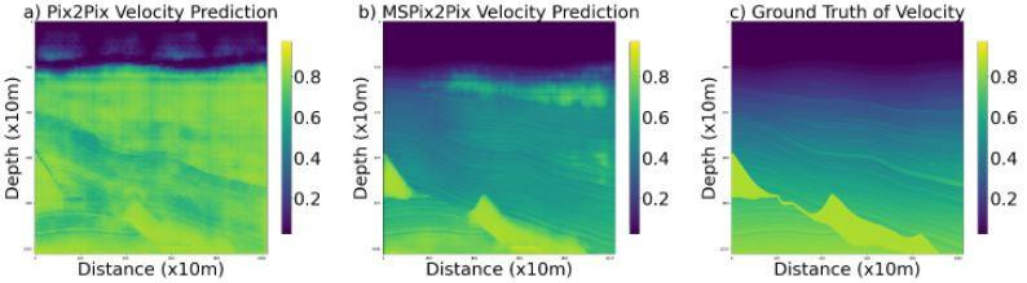

Figure 10 Velocity prediction results of Inline 1. Left: Prediction from pix2pix. Middle: Prediction from MS-pix2pix. Right: The ground truth. All displays are adjusted to the same scale

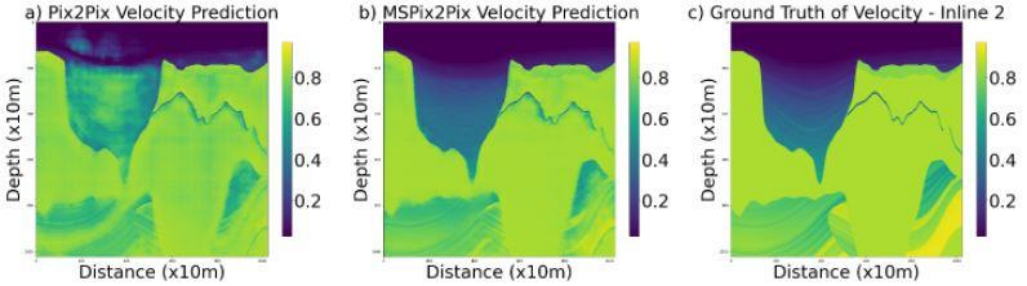

Figure 11 Velocity prediction results of Inline 2. Left: Prediction from pix2pix. Middle: Prediction from MS-pix2pix. Right: The ground truth. All displays are adjusted to the same scale

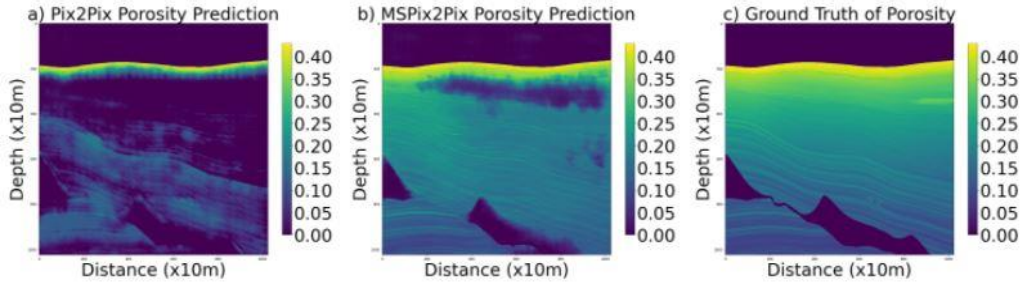

Figure 12 Porosity prediction results of Inline 1. Left: Prediction from pix2pix. Middle: Prediction from MS-pix2pix. Right: The ground truth. All displays are adjusted to the same scale

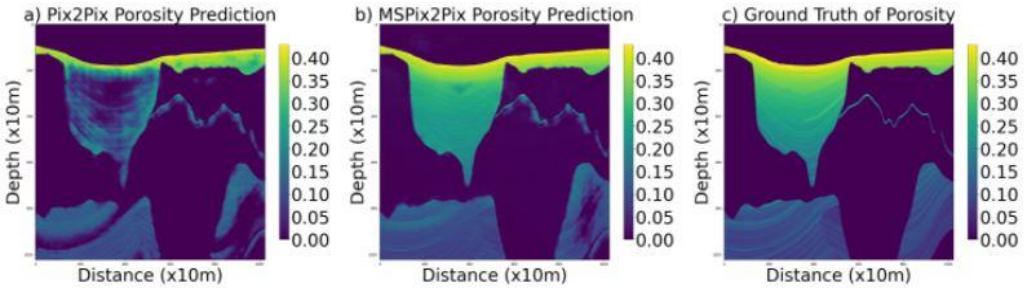

Figure 13 Porosity prediction results of Inline 2. Left: Prediction from pix2pix. Middle: Prediction from MS-pix2pix. Right: The ground truth. All displays are adjusted to the same scale

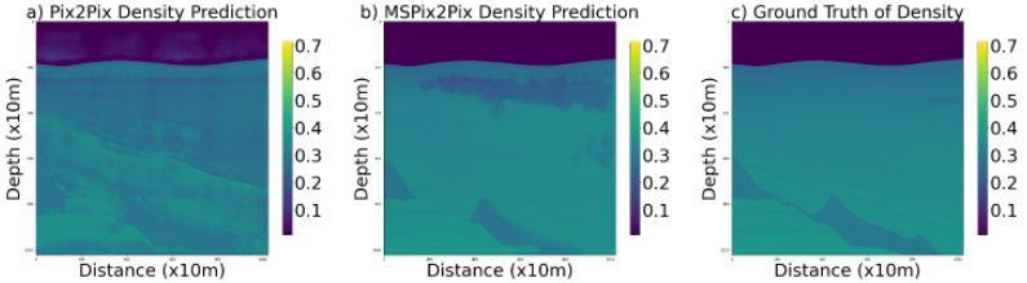

Figure 14 Density prediction results of Inline 1. Left: Prediction from pix2pix. Middle: Prediction from MS-pix2pix. Right: The ground truth. All displays are adjusted to the same scale

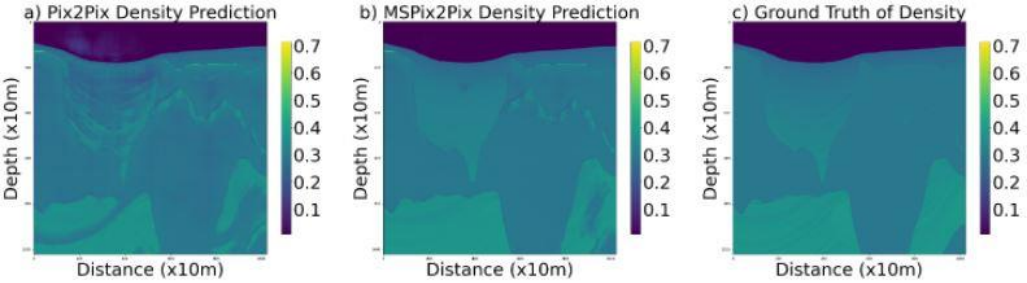

Figure 15 Density prediction results of Inline 2. Left: Prediction from pix2pix. Middle: Prediction from MS-pix2pix. Right: The ground truth. All displays are adjusted to the same scale

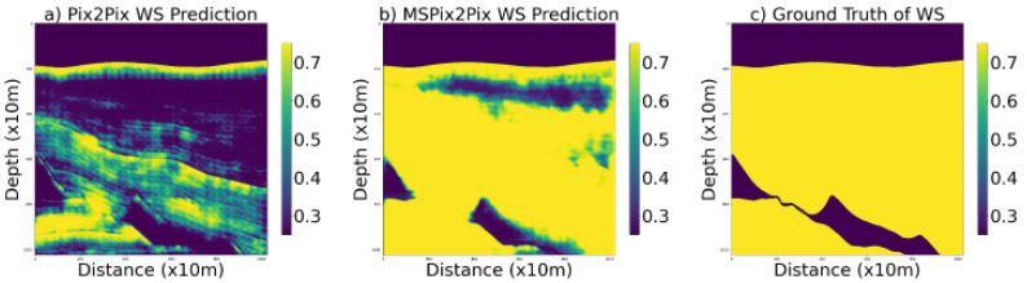

Figure 16 Water saturation prediction results of Inline 1. Left: Prediction from pix2pix. Middle: Prediction from MS-pix2pix. Right: The ground truth. All displays are adjusted to the same scale

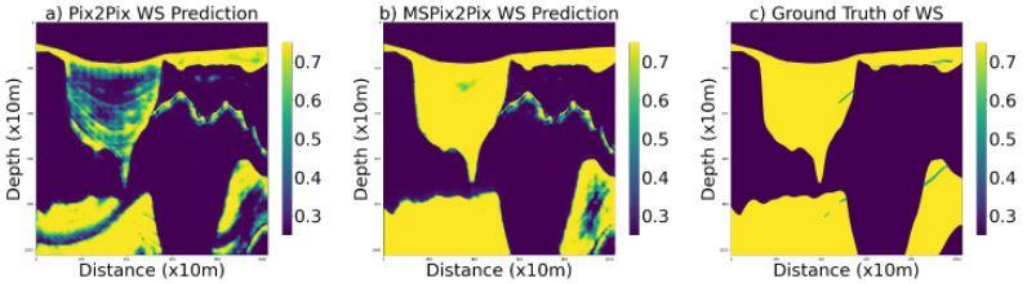

Figure 17 Water saturation prediction results of Inline 1. Left: Prediction from pix2pix. Middle: Prediction from MS-pix2pix. Right: The ground truth. All displays are adjusted to the same scale

Table 2 The prediction accuracy calculated using cross correlation and SSIM. The MS-Pix2Pix produces higher accuracy predictions for all properties and for all inlines

Properties	Cross correlation		SSIM	
Model	Pix2Pix	MS-Pix2Pix	Pix2Pix	MS-Pix2Pix
Velocity Inline 1	0.70	0.91	0.77	0.93
Velocity Inline 2	0.91	0.99	0.90	0.97
Porosity Inline 1	0.40	0.83	0.54	0.90
Porosity Inline 2	0.82	0.98	0.78	0.92
Density Inline 1	0.97	0.99	0.93	0.99
Density Inline 2	0.97	0.99	0.95	0.98
Water saturation Inline 1	0.43	0.84	0.76	0.95
Water saturation Inline 2	0.77	0.95	0.89	0.95

MS-Pix2Pix manages to produce predictions of higher accuracy as compared to the Pix2Pix network for all the subsurface properties. Although the predictions are better, there are still some areas that require further attention. In figure 10, 12, 14 and 16 for example, MS-Pix2Pix has improved the predictions of Pix2Pix by a lot. However, there is a wrong prediction that is predicted as salt body at the shallow depth. This could be due to the "dimmed" amplitude in the seismic data that resembles the salt body signature. In figure 17, although the prediction from MS-Pix2Pix is better, it is over predicted where there should not be a small body inside the salt area. As Pix2Pix is conditioned on the input image, the small body might be carried over from the input seismic.

6. Application on Field Data

Applying deep learning on a field data is a very challenging task due to two main reasons which are 1) the residual noise presence in the seismic data and 2) unavailability of the true label data. To test the robustness of our approach on a field data, we use seismic data from a Malaysian field with the labels generated by A. Fuad, M.I., et al [37] via rock physics guided deep learning-based properties inversion (Fig. 18).

The same workflow was applied to the field data such as normalization and transformation to 256x256 patches. The total number of patches is 512 of which 90% of them were used for training and the other 10% for validation. We repeated the same procedure for training which the best model from the first training was re-trained with a smaller kernel size of the discriminator. The best model from this was then used for testing. The testing data (Fig. 19) is a patch that was never used in the training and validation.

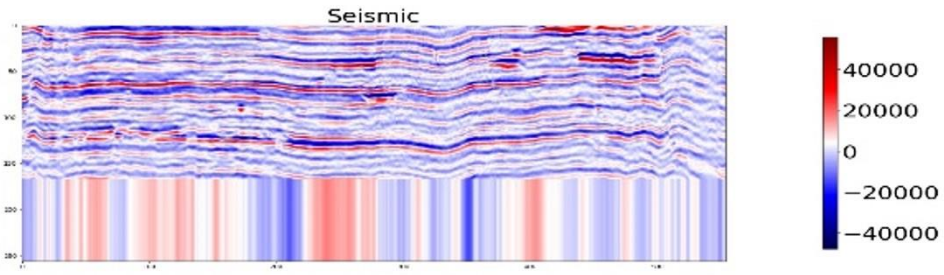

Figure 18 The seismic data of a Malaysian field. The last sample is repeated to that the z direction contains 256 samples.

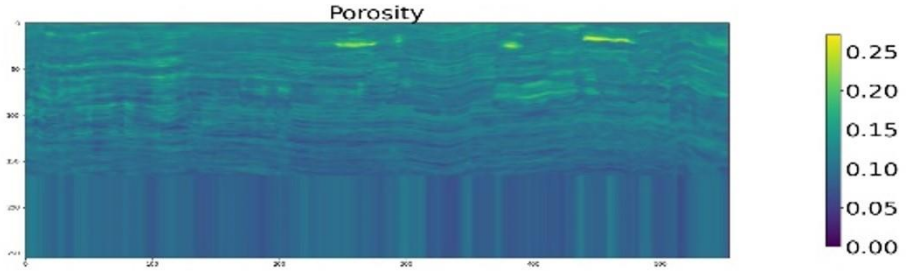

Figure 19 The corresponding label of porosity predicted by using DL based inversion guided by rock physics.

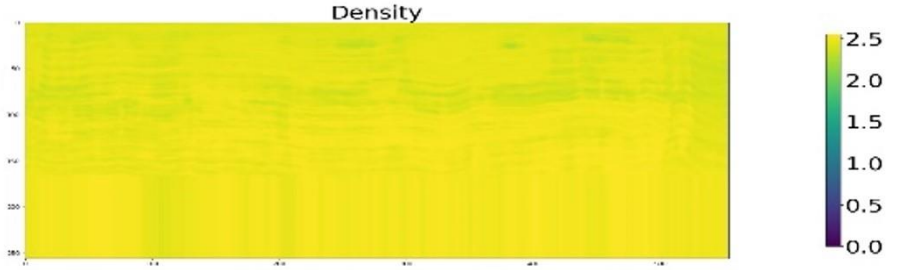

Figure 20 The corresponding label of density predicted by using DL based inversion guided by rock physics

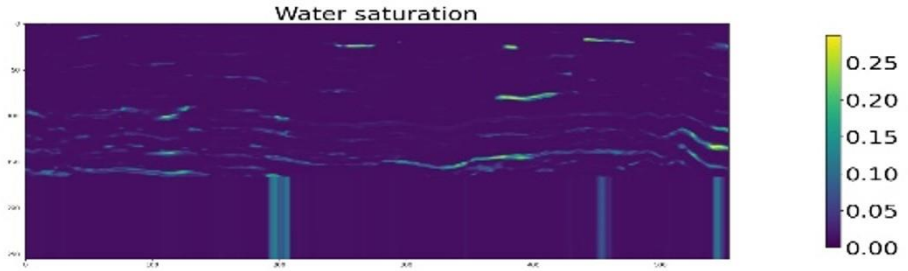

Figure 21 The corresponding label of water saturation predicted by using DL based inversion guided by rock physics

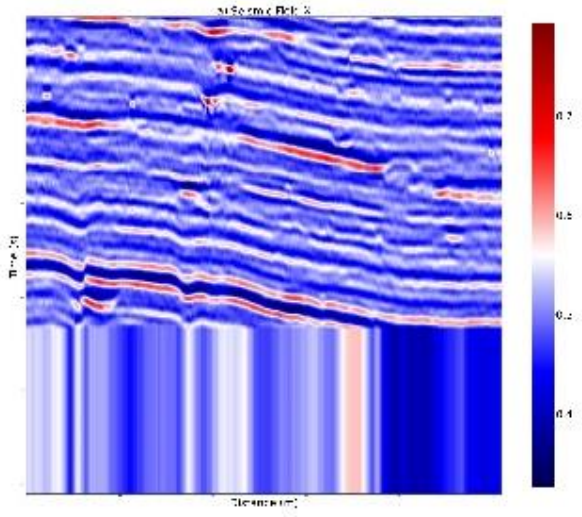

Figure 22 The seismic section used as the input data for testing.

Before examining the results in detail, let us look at the accuracy metric. Our objective here is to predict the value as close as possible to the real value. We then establish an accuracy metric that compares the value of each element with a 15% margin of error. We count the number of correct predictions and divide them with the total number of elements to get our final accuracy number.

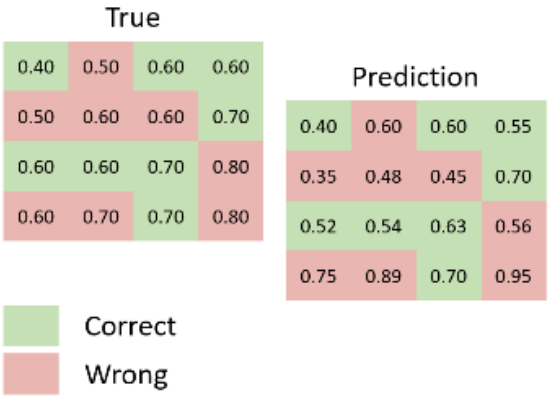

Figure 23 The accuracy metric. Element-wise comparison with 15% margin of error.

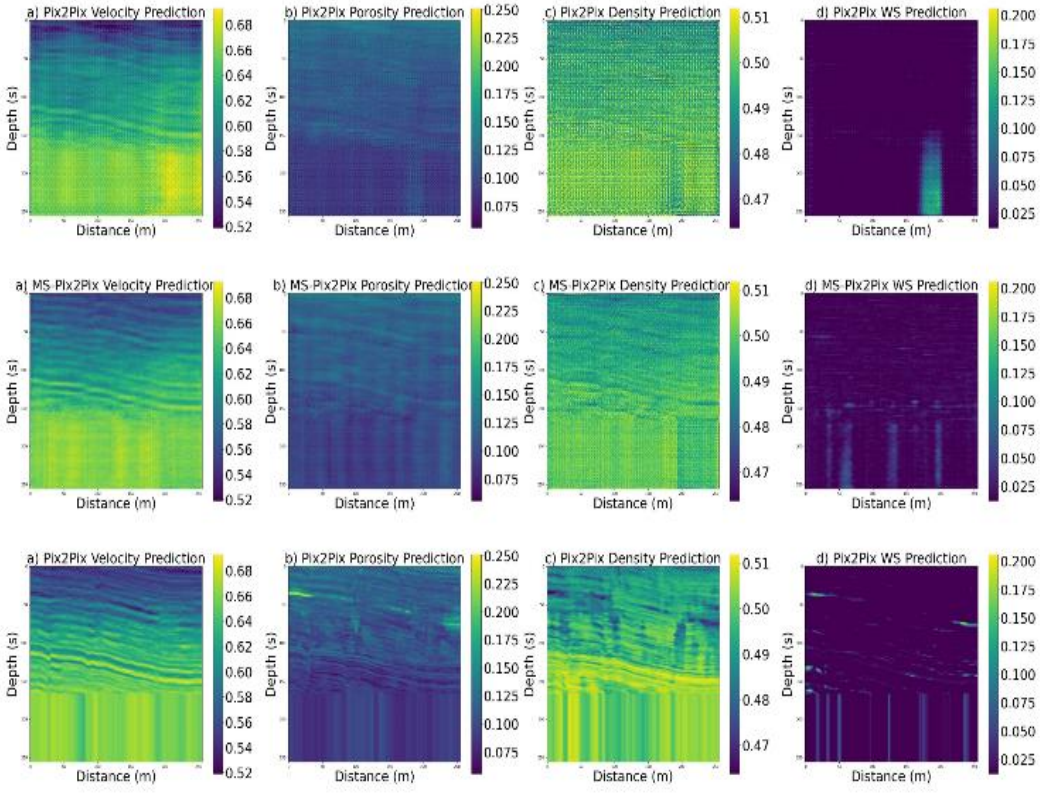

Figure 24 The field testing results. The first row is the results from the original Pix2Pix network. The second row is the results from MS-Pix2Pix, and the last row is the ground truth generated via deep learning-based properties inversion guided by rock physics.

Table 3 The prediction accuracy of the field data testing. MS-Pix2Pix manages to improve the prediction of the Pix2Pix network.

Properties	Pix2Pix	MS-Pix2Pix
P-velocity	99.7	99.9
Porosity	48.0	74.7
Density	99.6	99.9
Water saturation	0.05	0.24

In general, MS-Pix2Pix produces predictions of higher accuracy than the predictions coming from Pix2Pix network. MS-Pix2Pix manages to predict the velocity and density accurately. This would help in producing a better migrated images of the subsurface thus resulting in better interpretation of the geological features of the area. The porosity prediction is also improved in MS-Pix2Pix which can lead to a better delineation of the good reservoir rocks thus providing potential areas to be drilled. However, the prediction of the water saturation remains a challenge. More labels and higher training epochs could potentially overcome this limitation.

7. **Conclusion**

In this paper, we proposed multi-scale pix2pix (MS-Pix2Pix) as the network for transforming the seismic post stack to several subsurface properties such as velocity, porosity, density and water saturation. MS-Pix2Pix generates properties of higher accuracy and visual quality as compared to the original Pix2Pix as seen in the synthetic data testing (Table 2) and field data testing (Table 3). In addition, the use of the proposed method enables MS-Pix2Pix to predict several properties simultaneously with only one single network. However, although the results seem good, they can still be improved further.

Author Contributions: Conceptualization, M.A.I, A.H.A.L and E-H.T.W.; methodology, M.A.I.; validation, M.A.I.; formal analysis, M.A.I.; investigation, M.A.I.; data curation, M.A.I; M.I.A.F.; writing—original draft preparation, M.A.I; writing—review and editing, A.H.A.L, E-H.T.W, T.N.W.; supervision, A.H.A.L, E-H.T.W, E.E, M.S.; project administration, M.S. All authors have read and agreed to the published version of the manuscript.

Funding: The work is supported by PETRONAS Research Sdn Bhd through sponsorship of the main author for his post-graduate study at the Universiti Teknologi PETRONAS.

Institutional Review Board Statement: Not applicable

Informed Consent Statement: Not applicable

Data Availability Statement: Not applicable

Conflicts of Interest: The authors declare no conflict of interest.

References

1. Jones, I.F. Velocities, Imaging and Waveform Inversion: The Evolution of Characterising the Earth's Subsurface.; EAGE Publications, 2018
2. Virieux, J.; Operto, S. An Overview of Full-Waveform Inversion in Exploration Geophysics. *Geophysics* 74. 2009, wcc1-wcc26.
3. Xu, S.S.; Wang, D.; Chen, F L; Zhang, Y.; Lambaré, Gilles. Full Waveform Inversion for Reflected Seismic Data. 2012.
4. Berkhout, A. J. Combining Full Wavefield Migration and Full Waveform Inversion, a Glance into the Future of Seismic Imaging. *Geophysics* 77. 2012, S43-S50.
5. Verschuur, D. J.; Staal, X. R.; Berkhout, A. J. Joint Migration Inversion: Simultaneous Determination of Velocity Fields and Depth Images Using All Orders of Scattering. *The Leading Edge* 35. 2016, 1037-46.

6. Ishak, M.A., Verschuur, D.J. and Ghazali, A.R. A Hybrid Fwi-Jmi for High Resolution Velocity Estimation. 81st EAGE Conference and Exhibition 2019, London.
7. Grana, D.; Dvorkin, J.P. The Link between Seismic Inversion, Rock Physics, and Geostatistical Simulations in Seismic Reservoir Characterization Studies. *The Leading Edge* 30. 2011, 54-61.
8. Mavko, Gary; Mukerji, Tapan; Dvorkin, Jack Petrovich. The Rock Physics Handbook: Tools for Seismic Analysis of Porous Media. 1998.
9. Ahmad Fuad, M.I.; Ahmad Munif, H.A. Regional Rock physics implementation foe enhanced lithological and fluid predictions, a case study in deep reservoirs. Conference Proceedings, 81st EAGE Conference and Exhibition, 2019
10. Röth, G.; Tarantola, A. Neural Networks and Inversion of Seismic Data. *Journal of Geophysical Research: Solid Earth* 99. 1994, 6753-68.
11. Vladimir, K.; Oleg, O.; Tariq, A. Velocity Model Building by Deep Learning: From General Synthetics to Field Data Application. In *Seg Technical Program Expanded Abstracts 2020*, 1561-65
12. Hani, A.; Jeffrey, S. Seismic Velocity Model Building Using Neural Networks: Training Data Design and Learning Generalization. *Geophysics* 87. 2022, R193-R211.
13. Fangshu, Y.; Jianwei, M. Deep-Learning Inversion: A Next-Generation Seismic Velocity Model Building Method. *Geophysics* 84. 2019, R583-R99.
14. Araya-Polo, M.; Jennings, J.; Adler, A.; Dahlke, T. Deep-Learning Tomography. *The Leading Edge* 37. 2018, 58-66.
15. Martin, T.; Bell, M. An Innovative Approach to Automation for Velocity Model Building. *First Break* 37. 2019, 57-65.
16. Gao, Z.; Li, C.; Zhang, B.; Jiang, X.; Pan, Z.; Gao, J.; Xu, Z. Building Large-Scale Density Model Via a Deep-Learning-Based Data-Driven Method. *Geophysics* 86. 2020, M1-M15.
17. Das, V.; Pollack, A.; Wollner, U.; Mukerji, T. Effect of Rock Physics Modeling in Impedance Inversion from Seismic Data Using Convolutional Neural Network. *The 13th SEGJ International Symposium, Tokyo, Japan, 12–14 November 2018*. 2019
18. Das, V.; Mukerji, T. Petrophysical Properties Prediction from Prestack Seismic Data Using Convolutional Neural Networks. *Geophysics* 85. 2020, N41-N55
19. Weinzierl, W.; Wiese, B. Deep Learning a Poroelastic Rock-Physics Model for Pressure and Saturation Discrimination. *Geophysics* 86. 2021, MR53-MR66
20. Isola, P.; Zhu, J-Y.; Zhou, T.; Efros, A. A. Image-to-Image Translation with Conditional Adversarial Networks. *2017 IEEE Conference on Computer Vision and Pattern Recognition (CVPR)*. 2016, 5967-76.
21. Yunjey, C.; Min-je C.; Munyoung K.; Jung-Woo H.; Sunghun K.; Jaegul, C. Stargan: Unified Generative Adversarial Networks for Multi-Domain Image-to-Image Translation. *Proceedings of the IEEE Conference on Computer Vision and Pattern Recognition (CVPR)*. 2018, 8789-97
22. Karras, T.; Laine, S.; Aila, T. A Style-Based Generator Architecture for Generative Adversarial Networks. *2019 IEEE/CVF Conference on Computer Vision and Pattern Recognition (CVPR)*. 2018, 4396-405.
23. Ledig, C.; Theis, L.; Huszár, F.; Caballero, J.; Aitken, A.P.; Tejani, A.; Totz, J.; Wang, Z.; Shi, W. Photo-Realistic Single Image Super-Resolution Using a Generative Adversarial Network, *2017 IEEE Conference on Computer Vision and Pattern Recognition (CVPR)*. Honolulu, HI, USA, 2017, pp. 105-114
24. Wang, X.; Yu, K.; Wu, S.; Gu, J.; Liu, Y.; Dong, C.; Loy, C.C.; Qiao, Y.; Tang, Z. Esrgan: Enhanced Super-Resolution Generative Adversarial Networks. ECCV Workshops, 2018
25. Jiang, M.; Zhi, M.; Wei, L.; Yang, X.; Zhang, J.; Li, Y.; Wang, P.; Huang, J.; Yang, G. FA-GAN: Fused attentive generative adversarial networks for MRI image super-resolution. *Computerized medical imaging and graphics : the official journal of the Computerized Medical Imaging Society* 92. 2021
26. Zhang, K.; Hu, H.; Philbrick, K.; Conte, G.M.; Sobek, J.; Rouzrokh, P.; Erickson, B. SOUP-GAN: Super-Resolution MRI Using Generative Adversarial Networks. 2021
27. Cirillo, M.D.; Abramian, D.; Eklund, A. Vox2vox: 3d-Gan for Brain Tumour Segmentation. 2020
28. Skandarani, Y.; Jodoin, P-M.; Lalande, A. Gans for Medical Image Synthesis: An Empirical Study. *ArXiv* abs/2105.05318. 2021
29. Calimeri, F.; Marzullo, A.; Stamile, C.; Terracina, G. Biomedical Data Augmentation Using Generative Adversarial Neural Networks. 2017, 626-634
30. Kazeminia, S.; Baur, C.; Kuijper, A.; Ginneken, B.; Navab, N.; Albarqouni, S.; Mukhopadhyay, A. "Gans for Medical Image Analysis." *Artificial intelligence in medicine* 109.
31. Frid-Adar, M.; Diamant, I.; lang, E.; Amitai, M.M.; Goldberger, J.; Greenspan, H. Gan-Based Synthetic Medical Image Augmentation for Increased Cnn Performance in Liver Lesion Classification. *Neurocomputing* 321. 2018
32. Xiaoyang, R.L.; Nikolaos, M.; Ping, L.; Yuan, X.; Xing, Z. Seismic Compressive Sensing by Generative Inpainting Network: Toward an Optimized Acquisition Survey. *The Leading Edge* 38. 2019, 923-33
33. Liu, M.; Jervis, M.; Li, W.; Nivlet, P. Seismic Facies Classification Using Supervised Convolutional Neural Networks and Semi-supervised Generative Adversarial Networks. *Geophysics* 85. 2020, 047-58
34. Dupont, E.; Zhang, T.; Tilke, P.; Liang, L.; Bailey, W.J. Generating Realistic Geology Conditioned on Physical Measurements with Generative Adversarial Networks. *arXiv: Machine Learning*. 2018
35. Laloy, E.; Hérault, R.; Jacques, D.; Linde, N. Training-Image Based Geostatistical Inversion Using a Spatial Generative Adversarial Neural Network. *Water Resources Research* 54. 2017, 381-406

36. Prechelt, Lutz. Early Stopping - but When? In *Neural Networks: Tricks of the Trade*, edited by Genevieve B.; Müller Orr, Klaus-Robert, 1998, 55-69
37. Ahmad Fuad, M.I.; Jaya, M.S.; Abdrahman, S.; Lew, C.L.; Law, M. Deep Learning Based Seismic Elastic Properties Inversion Guided by Rock Physics. Paper presented at the ADIPEC, Abu Dhabi 2022.